On the theory of α(α')-β phase transitions of ordering type in niobium hydride

1989 J. Phys.: Condens. Matter 1 9085

(http://iopscience.iop.org/0953-8984/1/46/003)

J. Phys.: Condens. Matter 1 (1989) 9085–9100. Printed in the UK

On the theory of $\alpha(\alpha')$–β phase transitions of ordering type in niobium hydride

V G Vaks† and V I Zinenko‡

† I V Kurchatov Institute of Atomic Energy, Moscow 123182, USSR

‡ L V Kirensky Institute of Physics, Krasnoyarsk 660036, USSR

Received 4 October 1988

Abstract. Earlier methods for describing the statistical properties of hydrogen in the Nb-group metals are used to study the $\alpha(\alpha')$–β phase transitions in NbH_x and $\alpha(\alpha')$–δ in TaH_x and VD_x. We show that the observed broad range of concentrational stability for the ordered β or δ phase in these alloys can hardly be obtained in models with pairwise concentration-independent H–H interactions. However, this can naturally be explained if the concentrational anomalies in thermodynamic properties noted previously for the α phase in NbH_x are properly taken into account. The model of H–H interactions discussed earlier, complemented by two phenomenological mean-field parameters for the ordered β phase, enables us to describe the peculiar features of the experimental α–α'–β phase diagram in NbH_x. The calculated values of the order parameters, transition entropy and chemical potential of hydrogen in the β phase agree fairly well with available data. We predict anomalies in the thermodynamic and elastic properties of TaH_x and VD_x analogous to those observed in NbH_x.

1. Introduction

Investigations of thermodynamic properties and phase transitions (PT) of hydrogen in hydrides of the transition metals attract much attention. This is due to practical interest in the hydrides as well as to possible uses of these relatively simple systems for investigating general features of interactions and PT in interstitial alloys. Hydrides of the niobium-group metals are some of the most thoroughly studied; they have complex phase diagrams with a number of PT (Shober and Wenzl 1978, Somenkov and Shilstein 1980, Köbler and Welter 1982). Understanding the peculiar features of these diagrams can provide significant information on the nature and character of H–H interactions in metals. It is natural to start the consideration of ordered phases with the MX or Me–H structure, denoted as the β phase in NbH_x (or NbD_x) and as the δ phase in TaH_x (or TaD_x) and VD_x (see figure 1 and Shober and Wenzl (1978)). The structural basis for this phase is also characteristic for other H orderings in BCC hydrides. It is the main high-temperature ordered phase in the NbH_x-type hydrides at $0.7 < x < 1.1$. In addition, the cause for such a broad range of concentrational stability (the Me–H 'lattice crystal' is stable even at 30% of vacancies in the hydrogen sublattice) appears to be a significant qualitative problem for theory.

Theoretical models of the PT in NbH_x-type alloys were discussed by a number of authors, e.g. Horner and Wagner (1974), Futran *et al* (1982) and Hall *et al* (1987).

0953-8984/89/469085 + 16 $02.50

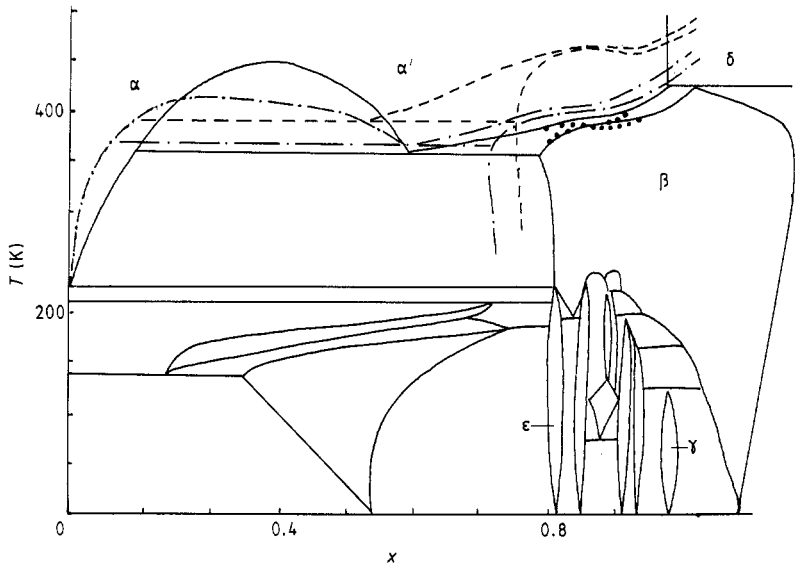

Figure 1. Phase diagram of the NbH_x system. Experiments: full curve, Shober and Wenzl (1978); full circles, Welter and Schöndube (1983). Calculations using the models described at the end of § 3: chain curve, model F; broken curve, model G.

However, most attention had been paid to the α–α' PT of the lattice gas–lattice liquid type. Calculations of the phase equilibrium curve $T_{\alpha\alpha'}(x)$ with the Monte Carlo method using the model with pairwise H–H interactions V_{HH} equal to the sum of the stress-induced ('elastic') term V_{si} and the strong repulsion (blocking) in the first three coordination spheres V_{sr} yielded a fair description of the observed $T_{\alpha\alpha'}(x)$ in NbH_x (Horner and Wagner 1974, Futran *et al* 1982). PT to the ordered β and ε phases in NbH_x were discussed by Hall *et al* (1987) only in the framework of a simplified model substituting an auxiliary tetragonal lattice for the real one of the interstitial sites in BCC Nb. For this model Hall *et al* concluded that the mentioned interactions $V_{HH} = V_{si} + V_{sr}$ cannot describe the PT corresponding to the β and ε orderings in NbH_x and additional long-range and non-pairwise interactions should be employed.

To calculate the statistical properties of alloys with strong inter-atomic interactions, such as hydrides, an analytic cluster field method (CFM) had been suggested in the papers of Vaks and Orlov (1986, 1988), Vaks and Zein (1987) and Vaks *et al* (1984, 1988a, b), to be referred to as I, II, III, IV, V and VI, respectively. The CFM is a simplified version of the known cluster variation method (Kikuchi 1951, De Fontaine 1979) which enables us adequately to take into account the strong long-range interactions, too. The lowest approximation of the CFM (that of the pair clusters) corresponds to the Richards (1983) method. In papers I–VI the CFM has been used for the consideration of a number of properties of NbH_x-type hydrides: the α–α' PT (II, VI); the symmetry of the ordered phases (I, III); short-range order effects (IV, V); thermodynamic properties in the disordered α phase (II); etc. In particular, estimates of the H–H interaction parameters made in II from the experimental data of Kuji and Oates (1984a) revealed a sharp concentration dependence of the partial enthalpy of hydrogen near $x = x_c \simeq 0.6$, which appears to reflect a significant change of the electronic state of hydrogen in NbH_x at this x. This illustrates the importance of band-structure effects in those alloys and agrees

qualitatively with the considerations of Hall *et al* (1987) on the significance of electronic and non-pairwise interactions in NbH_x.

In the present paper we use the methods and results of works I–VI to investigate the MX-type ordering in NbH_x, TaH_x and VD_x. We pay most attention to the $\alpha(\alpha')$–β PT in NbH_x, since it is the best studied experimentally. Comparison of the calculated phase equilibrium curves $T_{\alpha\beta}(x)$ with the observed ones confirms the previous estimates of the H–H interaction parameters (II) and enables us to generalise them to the β phase. We show, in particular, that the noted wide range of the β-phase stability noted is naturally explained by the sharp increase of $\mu(x)$ and $\partial\mu/\partial x$ in the α phase at $x \geqslant 0.6$. An analogous increase of $\mu(x)$ and $\partial\mu/\partial x$ in TaH_x and VD_x is predicted. The concentration and temperature dependences for a number of characteristics of the β phase are calculated: the order parameters ξ and ρ (defined in III), the chemical potential $\mu(x, T)$, the entropy of the PT $\Delta S(x)$, etc. The results agree satisfactorily with the available data. We also predict an anomalous softening for one of the shear constants in the α phase of VD_x near the transition temperature $T_\delta(x)$. On the whole the present study again reveals the importance of the non-pairwise, electronic effects in the hydrides and shows that all the main features of the PT under consideration can be understood in the framework of the concepts and models discussed in works I–VI.

2. Basic relations and methods of calculation

The model and calculation methods used are described in papers I and II. Let us give the main relations. In the hydrides considered the hydrogen atoms occupy tetrahedral interstitial sites in the BCC lattice of a metal, which form six equivalent sublattices denoted by index $p = 1, 2, 3, \bar{1}, \bar{2}, \bar{3}$ with the following basis vectors $\boldsymbol{\rho}_p$:

$$\boldsymbol{\rho}_1 = \tfrac{1}{4}\boldsymbol{a}_1 + \tfrac{1}{2}\boldsymbol{a}_2 \qquad \boldsymbol{\rho}_2 = \tfrac{1}{4}\boldsymbol{a}_2 + \tfrac{1}{2}\boldsymbol{a}_3 \qquad \boldsymbol{\rho}_3 = \tfrac{1}{4}\boldsymbol{a}_3 + \tfrac{1}{2}\boldsymbol{a}_1 \qquad \boldsymbol{\rho}_k = -\boldsymbol{\rho}_{\bar{k}} \tag{1}$$

where $\boldsymbol{a}_i$ is the translation vector along the main crystal axis i by the BCC lattice constant $a = |\boldsymbol{a}_i|$. In the disordered α phase all the sites are equivalent but in the MX phase there are three non-equivalent types of sites, which are denoted by index λ = a, b or α (see figure 2). The occupation numbers $n_p(\boldsymbol{R})$ for sublattices p in the BCC cell with centre $\boldsymbol{R}$ are related to the occupation numbers n_λ (for sites of type λ) as follows:

$$\begin{aligned} &n_3(\boldsymbol{R}) = n_{\bar{3}}(\boldsymbol{R}) = \tfrac{1}{2}(n_a + n_b) + \tfrac{1}{2}(n_a - n_b)\exp(\mathrm{i}\boldsymbol{k}_1 \cdot \boldsymbol{R}) \\ &n_1 = n_2 = n_{\bar{1}} = n_{\bar{2}} = n_\alpha \end{aligned} \tag{2}$$

where $k_1 = (1, 1, 0)\pi/a$. Equations (2) correspond to the presence in the MX phase of two concentration waves (Khachaturian 1974) with order parameters ξ and ρ connected with n_λ as

$$n_a = c(1 + 2\xi + 3\rho) \qquad n_b = c(1 + 2\xi - 3\rho) \qquad n_\alpha = c(1 - \xi) \tag{3}$$

where $c = x/6$ is the average occupation of sites in the MeH_x alloy. For perfect ordering we have $\xi = \rho = 1$, $n_a = x$, $n_b = n_\alpha = 0$.

Following II, we write the free energy F of the alloy (per Me atom) and the chemical potential μ of hydrogen in the form

$$F(x, T) = F_{\mathrm{conf}}(x, T) + E_{\mathrm{ci}}(x) + F_{\mathrm{ph}}(x, T) \tag{4a}$$

$$\mu(x, T) = \frac{\partial F}{\partial x} = \mu_{\mathrm{conf}}(x, T) + \mu_{\mathrm{ci}}(x) + \mu_{\mathrm{ph}}(x, T). \tag{4b}$$

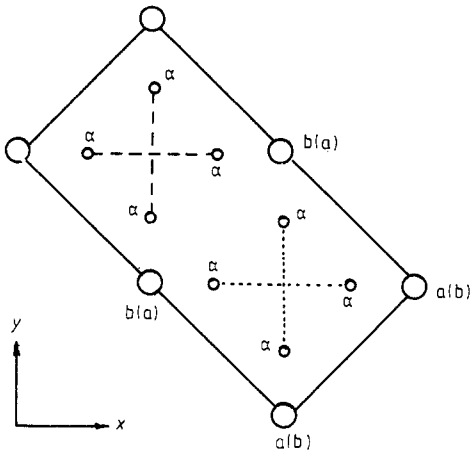

Figure 2. MX ordering in the BCC hydrides (see e.g. Shober and Wenzl 1978); for clarity, metal atoms are not shown. The large circles are tetrahedral interstitial sites in sublattices 3 and $\bar{3}$; the small circles are those in sublattices 1, $\bar{1}$, 2 and $\bar{2}$. The dotted and broken lines link the sites in the $z = 0$ and $z = \frac{1}{2}a$ planes, respectively; the indices a and b in or without parentheses are assigned to sites in the $z = \frac{1}{4}a$ or $z = \frac{3}{4}a$ planes, respectively, where a is the BCC lattice constant. In the case of perfect ordering, only the sites of type a are occupied. The structure is periodic in the $(\pm 1, \pm 1, 0)$ directions.

Here F_{conf} is the configurational contribution to F corresponding to energy and entropy of various distributions of protons over sites; E_{ci} is the configuration-independent term (including, in particular, the 'configurationally averaged' part of the band-structure energy); and F_{ph} is the phonon contribution. As in II, functions E_{ci} and F_{ph} are estimated from the experimental data (Kuji and Oates 1984a, b, Shapiro *et al* 1981) and F_{conf} is calculated as described in I and II. Interactions $V_{\text{HH}} = V(\boldsymbol{r})$ are supposed to be pairwise and F_{conf} has the form

$$F_{\text{conf}} = -(1/N)T \ln \sum_{\{\hat{n}_r\}} \exp(-\beta \hat{H}_{\text{conf}}) \tag{5a}$$

$$\hat{H}_{\text{conf}} = \tfrac{1}{2} \sum_{r \neq r'} V(\boldsymbol{r} - \boldsymbol{r}') \hat{n}_r \hat{n}_{r'}. \tag{5b}$$

Here $\beta = 1/T$, N is the total number of Me atoms, the operator $\hat{n}_r$ being equal to 0 and 1 describes the occupation of a site $\boldsymbol{r}$ by a proton and the sum in (5*a*) is taken over all the sets of occupation numbers $\hat{n}_r$.

In the cluster approximation denoted in I as 8s approximation the thermodynamic contributions of interactions $V(\boldsymbol{r}_i) = V_i$ in the first, second and third coordination spheres are described with the use of eight-site and three-site clusters and those of interactions V_i with $i \geqslant 4$ with pair clusters. In the β phase the free energy $F_{\text{conf}} = F_\beta$ and chemical potentials of sublattices μ_λ^β have the form

$$F_\beta = F_\beta^{\text{s}} + F_\beta^{\text{mf}} + F_\beta^{\text{c}} \tag{6a}$$

$$\mu_\lambda^\beta = \frac{1}{\nu_\lambda} \frac{\partial F_\beta}{\partial n_\lambda} = \mu_\lambda^{\text{s}} + \mu_\lambda^{\text{c}} + \mu_\lambda^{\text{mf}}. \tag{6b}$$

Here ν_λ is the number of sites of type λ per Me atom ($\nu_{\text{a}} = \nu_{\text{b}} = 1$, $\nu_\alpha = 4$); F_β^{s} and μ_λ^{s} are the contributions of the short-range interactions V_1, V_2, V_3 and of terms with the configurational entropy; F_β^{mf} and μ_λ^{mf} are the contributions of the rest of the constants $V_{i \geqslant 4}$ taken in the mean-field approximation; and F_β^{c} and μ_λ^{c} are the 'correlative' contributions of V_i from the fourth to the eighteenth coordination spheres described in the pair cluster approximation (I).

In calculating F_β^{s} and μ_λ^{s}, the interactions V_1 and V_2 are supposed to be repulsive and very large ('blocking'), V_1, $V_2 \gg T$, while V_3 is finite (II). Then the explicit

expressions for the short-range contributions F^s, μ^s and Ω^s to F_β, μ_λ^β and the thermodynamic potential $\Omega = F - \mu x$ in terms of the sublattice occupation numbers n_λ are as follows (I):

$$F_\beta^s = \Omega^s + \sum_\lambda \nu_\lambda \mu_\lambda^s n_\lambda \tag{7a}$$

$$\Omega^s = T \ln\left(\frac{p_{\mathrm{ab}\alpha\alpha}^2 p_{\alpha\alpha\alpha\alpha} (p_{\mathrm{a}\alpha\alpha} p_{\mathrm{b}\alpha\alpha} p_{\mathrm{ab}\alpha}^2 p_{\alpha\alpha\alpha}^2)^{-1}}{(1+\xi_\mathrm{a})(1+\xi_\mathrm{b})(1+\eta)^2(1+\zeta)^2}\right) \tag{7b}$$

$$\mu_\alpha^s \times \tfrac{1}{2} T \ln\left(\frac{\xi_\mathrm{a}\zeta_\mathrm{b}\eta^2(1+\xi_\mathrm{a})(1+\xi_\mathrm{b})(1+\eta)(1+\zeta)^3 p_{\mathrm{a}\alpha\alpha} p_{\mathrm{b}\alpha\alpha} p_{\mathrm{ab}\alpha} p_{\alpha\alpha\alpha}^3}{16 n_\alpha^2 (1+e_3\xi_\mathrm{a})(1+e_3\xi_\mathrm{b})(1+e_3\zeta)^2 p_{\mathrm{ab}\alpha\alpha}^2 p_{\alpha\alpha\alpha}^2}\right) \tag{7c}$$

$$\mu_\mathrm{a}^s = T \ln\left(\frac{n_\mathrm{a}\zeta^2(1+\xi_\mathrm{a})(1+\eta)^2 p_{\mathrm{a}\alpha\alpha} p_{\mathrm{ab}\alpha}^2}{n_{\mathrm{ab}}^2 (1+e_3\eta)^2 p_{\mathrm{ab}\alpha\alpha}^2}\right) \tag{7d}$$

and μ_b^s is obtained from μ_a^s by interchanging indices a $\leftrightarrow$ b. In equations (7*a–d*) we use the notation

$$n_{ij\ldots k} = n_i + n_j + \ldots + n_k \qquad p_{ij\ldots k} = 1 - n_{ij\ldots k} \qquad e_3 = \exp(-\beta V_3)$$

$$\xi_\mathrm{a} = \frac{4n_\alpha}{R_\mathrm{a} + p_{\mathrm{a}\alpha\alpha\alpha}} \qquad \eta = \frac{4n_\alpha}{R_1 + q_+} \qquad \zeta = \frac{2n_{\mathrm{ab}}}{R_2 + q_-}$$

$$q_\pm = p_{\mathrm{ab}\alpha\alpha} \pm e_3(n_{\mathrm{ab}} - 2n_\alpha) \qquad R_\mathrm{a} = (p_{\mathrm{a}\alpha\alpha\alpha}^2 + 8e_3 n_\alpha p_{\mathrm{a}\alpha\alpha})^{1/2}$$

$$R_1 = (q_+^2 + 8e_3 n_\alpha p_{\alpha\alpha\alpha})^{1/2} \qquad R_2 = (q_-^2 + 4e_3 n_{\mathrm{ab}} p_{\mathrm{ab}\alpha})^{1/2}$$

and ξ_b is obtained from ξ_a by interchanging a and b.

The mean-field contributions F_β^{mf} and $\mu_\lambda^{\mathrm{mf}}$ are (I)

$$F_\beta^{\mathrm{mf}} = 6c^2(\tfrac{1}{2}\gamma_\alpha + \xi^2\gamma_\xi + \tfrac{3}{2}\gamma_\rho) \tag{8a}$$

$$\mu_\mathrm{a}^{\mathrm{mf}} = c(\gamma_\alpha + 2\xi\gamma_\xi + 3\rho\gamma_\rho) \qquad \mu_\mathrm{b}^{\mathrm{mf}} = c(\gamma_\alpha + 2\xi\gamma_\xi - 3\rho\gamma_\rho)$$

$$\mu_\alpha^{\mathrm{mf}} = c(\gamma_\alpha - \xi\gamma_\xi) \tag{8b}$$

where γ_i are the mean-field constants discussed in V.

The correlative contribution F_β^c or μ_λ^c are defined as the differences between contributions of interactions V_i to F_β or μ_λ calculated in the pair cluster approximation and that in the mean-field one:

$$F_\beta^c = \tfrac{1}{2}\sum_{\lambda\rho} \nu_\lambda \sum_{i=4}^{18} m_i^{\lambda\rho} F_{i,\lambda\rho}^c \qquad \mu_\lambda^c = \sum_\rho \sum_{i=4}^{18} m_i^{\lambda\rho} \mu_{i,\lambda\rho}^c \tag{9}$$

where quantities $F_{i,\lambda\rho}^c$ and $\mu_{i,\lambda\rho}^c$ are given by

$$\beta F_{i,\lambda\rho}^c = 2n_\lambda \ln(1 - n_\rho g_i^{\lambda\rho}) - \ln(1 - n_\lambda n_\rho g_i^{\lambda\rho}) - n_\lambda n_\rho \beta V_i \tag{10a}$$

$$\beta\mu_{i,\lambda\rho}^c = \ln(1 - n_\rho g_i^{\lambda\rho}) - n_\rho \beta V_i \tag{10b}$$

$$g_i^{\lambda\rho} = \frac{2f_i}{1 + (n_\lambda + n_\rho)f_i + R_{i,\lambda\rho}} \qquad f_i = \exp(-\beta V_i) - 1 \tag{10c}$$

$$R_{i,\lambda\rho} = [(1 + n_\lambda f_i + n_\rho f_i)^2 - 4n_\lambda n_\rho f_i(1 + f_i)]^{1/2} \tag{10d}$$

and $m_i^{\lambda\rho}$ in (9) is the number of sites of type ρ in the ith coordination sphere of site λ;

Table 1. Coordination numbers $m_i^{\lambda\nu}$ in (9) and values of interaction constants $V_i = V(r_i)$ used for NbH_x.

i	$4r_i/a$	m_i	m_i^{aa}	m_i^{ab}	$m_i^{a\alpha}$	$m_i^{\alpha\alpha}$	V_i (K)
1	101	4	0	0	4	2	∞
2	002	2	0	2	0	2	∞
3	211	8	0	0	8	4	800
4	220	4	2	2	0	4	33
5	301	8	0	0	8	4	−127
6	222	8	4	4	0	8	−224
7	123	16	0	0	16	8	−130
8a	004	2	2	0	0	2	−483
8b	400	4	0	4	0	4	83
9a	033	4	0	0	4	2	259
9b	141	8	0	0	8	4	300
10a	402	4	4	0	0	4	−182
10b	042	4	4	0	0	4	552
11	323	8	0	0	8	4	−114
12	224	8	4	4	0	8	25
13a	501	8	0	0	8	4	41
13b	413	16	0	0	16	8	47
15	251	16	0	0	16	8	84
16a	404	8	0	8	0	8	86
16b	440	4	4	0	0	4	−56
17a	053	8	0	0	8	4	87
17b	433	8	0	0	8	4	−74
18a	006	2	0	2	0	2	−110
18b	442	8	0	8	0	8	−95

$m_i^{\lambda\rho}$ obeys the relation $\nu_\lambda m_i^{\lambda\rho} = \nu_\rho m_i^{\rho\lambda}$. The values of $m_i^{aa} = m_i^{bb}$, m_i^{ab}, $m_i^{a\alpha} = m_i^{b\alpha}$, $m_i^{\alpha\alpha}$ and the total $m_i = m_i^{\lambda a} + m_i^{\lambda b} + m_i^{\lambda\alpha}$ values are presented in table 1.

The H–H interaction constants V_i were estimated in II in the model (denoted 'model A') in which V_{HH} is the sum of the stress-induced term V_{si}, the anharmonic repulsion in the first three coordination spheres V_{sr} and the screened Coulomb ('electronic') interaction of protons V_e. The values of V_i in that model are presented in table 1. The corresponding mean-field constants γ_i in (8) were calculated in V and are (in K)

$$\gamma_\alpha = -13\,320 \qquad \gamma_\xi = -2580 \qquad \gamma_\rho = -220. \tag{11}$$

As discussed in II, this simple model with pairwise V_i for the α phase of NbH_x gives a fair description of both the α–α' phase diagram and the observed temperature dependences of the 'excess' chemical potential

$$\mu^E = \mu(x, T) - \mu_{id}(x, T) \tag{12}$$

where μ_{id} is the chemical potential for the ideal solution (Kuji and Oates 1984a). However, to describe the concentration dependences, in particular the sharp increase of μ and $\partial\mu/\partial x$ at $x \geqslant 0.6$, one must take into consideration the mentioned configuration-independent (or 'band') contribution $E_{ci}(x)$ in (4). The total temperature-independent contribution h_{ti}^E to μ^E,

$$h_{ti}^E(x) = \mu_{ci}^E(x) + \mu^{mf}(x) \tag{13}$$

has been estimated from the experiments of Kuji and Oates (1984a) and is given by formula (29b) and figure 2 in II. This $h_{ti}^E(x)$ will be denoted as $h_\alpha(x)$. For larger $x > 0.83$,

formula (29b) and figure 2 in II. This $h_{ti}^{E}(x)$ will be denoted as $h_\alpha(x)$. For larger $x > 0.83$, which were not investigated by Kuji and Oates (1984a), the values of $h_{ti}^{E}(x)$ will be estimated below from the analogous data of Kuji and Oates (1984b) for the β phase.

Lastly, in treating the phonon contribution F_{ph} in (4), we suppose that the changes of the phonon spectra at the α'–β PT are small (Shapiro *et al* 1981). Therefore, we describe F_{ph} by the same expressions as for the α phase. They are given by formulae (4) and (2*b*) in II and have been obtained by an interpolation of the concentration dependence of the phonon spectra observed in the α phase.

The equilibrium values of the order parameters ξ and ρ in the β phase at given T and x can be found from the condition of equality of the sublattice chemical potentials $\mu_a = \mu_b = \mu_\alpha$ or from the equivalent condition of minimum of the free energy $F_\beta(T, x, \xi, \rho)$ over ξ and ρ. The latter turns out to be more convenient for calculations. Thus we find equilibrium $\xi = \xi_m$ and $\rho = \rho_m$, minimising in the range $0 \leqslant \xi, \rho \leqslant 1$ on a mesh with steps $\Delta\xi \leqslant 0.01$ and $\Delta\rho \leqslant 0.01$.

The curves of the phase equilibrium α–β (or α'–β) are obtained from the equations

$$\mu^\alpha(T, x_\alpha) = \mu_a^\beta(T, x_\beta, \xi_m, \rho_m) \tag{14a}$$

$$\Omega_\alpha(T, x_\alpha) = \Omega_\beta(T, x_\beta, \xi_m, \rho_m). \tag{14b}$$

Here index α or β indicates that μ or Ω is calculated for the α or β phase, $\Omega_i = F_i - x_i\mu^i$, $x_\alpha = x_\alpha(T)$ and $x_\beta = x_\beta(T)$ are the solutions of equations (14) which determine the left and right boundary of the two-phase region $\alpha + \beta$ in the (x, T) phase diagram. The phase equilibrium curve α–α' (of the gas–liquid type) is determined by equation (13) on replacing $\beta \to \alpha'$ and $\xi_m = \rho_m = 0$.

3. α–α'–β phase diagrams and the chemical potential of hydrogen in the β phase

On discussing the calculated α–α'–β phase diagrams, we first note that direct use of model A described above with the V_i values from table 1 and γ_i from equations (11) leads to the wrong description of the symmetry of the ordered β phase. Instead of the MX phase with order parameters $\xi \neq 0$, $\rho \neq 0$, a partly ordered phase with $\xi \neq 0$, $\rho = 0$ (called the ξ phase in III and below) emerges and remains stable down to rather low $T \sim 50$ K. The analysis in V has shown that such suppression of the concentration wave (CW) ρ, i.e. a large value of the stiffness $S_\rho = \partial^2 F/\partial\rho^2$ for this CW, is mainly due to an anomalous smallness of the mean-field constant γ_ρ in (11) in the given model, while the short-range and correlative contributions to S_ρ have the same order of magnitude as those for the soft CW ξ (the correlative terms being small). Such a smallness of γ_ρ is characteristic of both the stress-induced interaction V_{si} and the electronic one V_e. Since V_{si} is estimated from the experimental data (II), the error is evidently connected with V_e. It shows that our simple model for V_e with linear screening of protons in a homogeneous electron liquid is insufficient for the description of the CW ρ characteristics, and that the disregarded effects of the band structure, of the inhomogeneous screening by d-electrons, of the higher orders in the electron–proton interaction, etc., are important. At the same time, the stiffness for the CW ξ (which is dominated by the stress-induced interaction V_{si}; see V) seems to be estimated realistically in our model. This is implied by a reasonable agreement of our calculated 'ordering spinodals' $T_\xi(x)$ (the temperatures at which the disordered α phase becomes unstable with respect to the creation of the ξ

CW) with that estimated from the experiments (see V and figure 8 of this paper) as well as by the estimates of γ_ξ from the experimental phase diagram discussed below.

In connection with the above, we suppose that in describing the main features of the α–β PT, we can simulate all the disregarded effects by a simple change of the mean-field constants γ_ρ and γ_ξ, compared to the model estimate (11), while the rest of the contributions F_β^s, F_β^c in (6) can still be taken from the model calculations. This can be understood, for example, as an addition to F_β and μ^β of the ordering-dependent band-structure contributions analogous to the configuration-independent terms E_{ci} and μ_{ci} in (4) and (12). The values of γ_ρ and γ_ξ will be estimated from fitting to the observed phase diagram, while the comparison with experiments of the calculated temperature and concentration dependences for various characteristics will allow us to appreciate the adequacy of the model.

The phase diagrams calculated with various γ_ρ, γ_ξ and $h_{ti}^E(x)$ in (13) are presented in figures 3(*a*)–(*d*). Let us discuss these results. Figure 3(*a*) illustrates the sensitivity of the phase diagram to the γ_i values. The curves presented correspond to $|\gamma_\rho| < |\gamma_\xi|$ and $\gamma_\rho \sim \gamma_\xi$. If the difference $\Delta\gamma = |\gamma_\xi| - |\gamma_\rho|$ increases, the above-mentioned ξ phase emerges even at relatively low $\Delta\gamma$. For example, the calculations (not presented in figure 3) show that at $\gamma_\xi = -2400$ K, $\gamma_\rho = -1700$ K the ξ phase appears already at $T = 390$ K, $x_\beta = 0.56$. Figures 3(*a*) and 1 also show that at $\gamma_\xi = \gamma_\xi^0 = -2200$ K, $\gamma_\rho = \gamma_\rho^0 = -1850$ K the calculated triple point $x_t = 0.52$, $T_t = 370$ K is close to the experimental one, while for $\gamma_\xi = \gamma_\xi^1 = -2300$ K, $\gamma_\rho = \gamma_\rho^1 = -2200$ K the values of x_t and T_t are displaced from it. However, the models with $\gamma_i = \gamma_i^1$ are better at describing the experimental values of the transition entropy ΔS; see figure 7. Thus, in the estimates below we use both $\gamma_i = \gamma_i^0$ and $\gamma_i = \gamma_i^1$.

Figure 3(*b*) illustrates an important result of the effect of the configuration-independent terms E_{ci} and μ_{ci} in (4) and (13) on the PT. It shows that, when these terms are absent and the H–H interactions are purely pairwise, the concentration interval of the β phase stability near the stoichiometric value $x = 1$ is very narrow: for all the γ_i and T values considered, $x(T)$ varies from 0.975 to 0.995; in figure 3(*b*) they are equal to unity within the accuracy of the drawing. This narrowness of the stability for the ordered phase, i.e. for the 'lattice crystal', corresponds to the well known smallness of the equilibrium concentration of vacancies in the actual crystals and is apparently characteristic of all the models of alloys with purely pairwise interactions of interstitial atoms. At the same time, comparison of figures 3(*a*) and (*b*) shows that the observed large number of 'vacancies' in the β phase of NbH_x is naturally explained when the non-pairwise contribution $E_{ci}(x)$ (estimated from the experiments of Kuji and Oates (1984a)) is taken into account.

To elucidate this and other features of the phase diagrams of the NbH_x-type systems, we consider relations between thermodynamic potentials of the α' and β phases on their phase equilibrium curves. Differentiating equation (14*b*) over T and using (14*a*) we obtain

$$S_{\alpha'} - S_\beta = (x_\beta - x_{\alpha'})\left[\frac{(\partial\mu_{\alpha'}/\partial x)_T}{(\mathrm{d}T_{\alpha'}/\mathrm{d}x)} + \left(\frac{\partial\mu_{\alpha'}}{\partial T}\right)_x\right]$$

$$= (x_\beta - x_{\alpha'})\left[\frac{(\partial\mu_\beta/\partial x)_T}{(\mathrm{d}T_\beta/\mathrm{d}x)} + \left(\frac{\partial\mu_\beta}{\partial T}\right)_x\right]. \tag{15}$$

Here $S_i = S(x_i, T) = -\partial F_i/\partial T$ is the entropy per Me atom in phase i on the phase

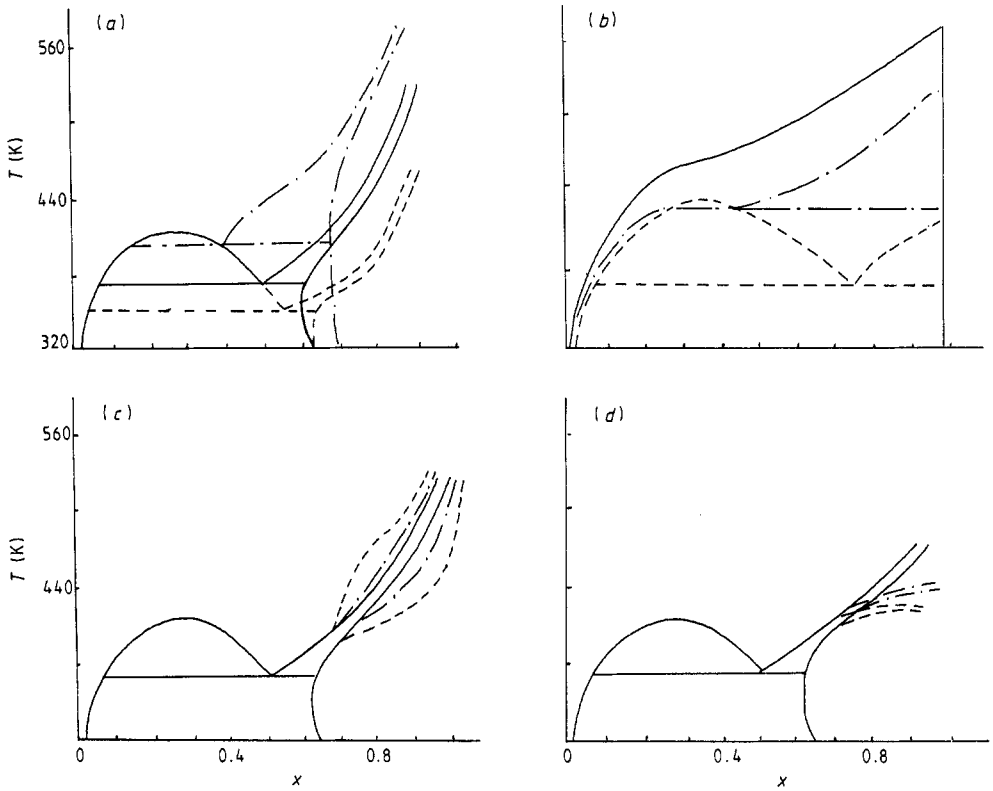

Figure 3. The α–α'–β phase diagram for NbH_x for different forms of $h_{ti}^{E}(x)$ in (13) and values of γ_ξ, γ_ρ in (8) (in K). (*a*) Here $h_{ti}^{E}(x)$ denotes $h_\alpha(x)$ determined from experiments of Kuji and Oates (1984a) in II. The full curve corresponds to $\gamma_\xi = \gamma_\xi^0 = -2200$, $\gamma_\rho = \gamma_\rho^0 = -1850$; the chain curve to $\gamma_\xi = -2300$, $\gamma_\rho = -2200$; the broken curve to $\gamma_\xi = 1900$, $\gamma_\rho = -1800$. (*b*) Here $h_{ti}^{E}(x)$ stands for the mean-field expression $\mu^{mf}(x) = \gamma_\alpha x$, $\gamma_\alpha = -13320$. The full curve corresponds to $\gamma_\xi = \gamma_\xi^0$, $\gamma_\rho = \gamma_\rho^0$; the chain curve to $\gamma_\xi = -1900$, $\gamma_\rho = -1800$; the broken curve to $\gamma_\xi = \gamma_\rho = -1600$. (*c*) Here $\gamma_\xi = \gamma_\xi^0$, $\gamma_\rho = \gamma_\rho^0$, $h_{ti}^{E}(x)$ is taken from (16). The full curve corresponds to $A = 10^4$ in (16); the chain curve to $A = 5 \times 10^4$; the broken curve to $A = 7 \times 10^4$. (*d*) Here $h_{ti}^{E}(x)$ is taken from (18); $\gamma_i(x)$ from (19) with $d_i = 0$, $\gamma_\xi = \gamma_\xi^0$, $\gamma_\rho = \gamma_\rho^0$, $b_\xi = b_\rho = b$. The full curve corresponds to b from (19) being 2000; the chain curve to $b = 3000$; the broken curve to $b = 4000$.

equilibrium curve $x_i(T)$ or $T_i(x)$. Equation (15) enables us to make qualitative conclusions on peculiarities of the phase diagrams in the case when μ_i and $\partial\mu_i/\partial x$ vary sharply with x, as occurs in NbH_x at $x \geqslant 0.6$. According to (4) and (6), the entropy S_i is the sum of the short-range, correlative and phonon contributions. Each of them varies slowly with x at $x \sim x_{\alpha'}$ or $x \sim x_\beta$ within any reasonable theoretical model, as well as in the estimates from experiments (II, Kuji and Oates 1984a). The same is also true for terms $\partial\mu_i/\partial T$ in (15). Therefore, high values of $\partial\mu_i/\partial x$ in (15) must be compensated by a smallness of the predicted $(x_\beta - x_{\alpha'})(\mathrm{d}T_i/\mathrm{d}x)^{-1}$. However, the value of $\mathrm{d}T_i/\mathrm{d}x$ cannot be too large. $T_{\alpha'}(x)$ or $T_\beta(x)$ are starting temperatures for the PT at decreasing or increasing T and their values are determined by the gain of free energy $\Delta F = F_\beta - F_\alpha$ on ordering. In accepted models of the ordering, ΔF varies smoothly with x. This is confirmed also in measurements of hydrogen solubility in the α and β phases (Kuji and Oates 1984a, b). Thus both in our calculations and in experiments the values of $\mathrm{d}T_i/\mathrm{d}x$

in NbH_x-type hydrides are not large (see figure 1 and Shober and Wenzl (1978)). Therefore, at high values of $\partial\mu/\partial x$, equation (15) can be satisfied only with small values of $x_\beta - x_{\alpha'}$. These thermodynamic considerations appear to explain the mentioned stability of the MX structure in NbH_x, TaH_x and VD_x even at very large number of vacancies as well as the narrowness over x of the coexistence region $\alpha' + \beta$ or $\alpha' + \delta$ in these hydrides (Shober and Wenzl 1978). Therefore, we expect that the sharp increase of $\mu(x)$ and $\partial\mu/\partial x$ at $x \geqslant 0.6$ observed in NbH_x does also occur in TaH_x and VD_x. Experimental verifications of this prediction seem to be rather interesting.

The considerations about the connection between the smallness of $x_\beta - x_{\alpha'}$ and large values of $\partial\mu/\partial x \simeq \partial h_{ti}/\partial x$ are also illustrated in figure 3(*c*). Here we show the results of calculations of $T_i(x)$, in which for $h_{ti}^E(x)$ in (13) we use not $h_\alpha(x)$ from II but smoother expressions of the form

$$h_{ti}^E(x) = h_\alpha(x) - A(x - 0.7)^2\theta(x - 0.7) \tag{16}$$

where $\theta(x)$ is zero for $x < 0$ and unity for $x > 0$. Comparing figures 3(*c*) and (*a*), we see that the decrease of $\partial h_{ti}^E/\partial x$ really extends the coexistence region $\alpha' + \beta$, and this extension is significant for $A \geqslant 5 \times 10^4$ K.

Let us now compare the model phase diagram in figure 3(*a*) with the experimental one in figure 1. On the whole the simple model used in figure 3(*a*) satisfactorily describes the observed α–α'–β diagram. There is, however, a qualitative disagreement for large $x > 0.7$: the experimental $T_i(x)$ curves show an inflection point here and become almost horizontal, while the calculated ones continue to increase with a positive curvature. The disagreement may be due to two factors not yet discussed: (i) inapplicability of the extrapolation of the function $h_{ti}^E(x) = h_\alpha(x)$ to large $x > 0.83$, not studied by Kuji and Oates (1984a); (ii) a possible concentration dependence of ordering-dependent interactions, in particular, of the parameters $\gamma_i = \gamma_i(x)$. Let us discuss these factors.

To estimate $h_{ti}^E(x)$ at large x, we use the data obtained by Kuji and Oates (1984b) on $\mu^E(x, T)$ in the β phase. These authors interpolated their results with the expression

$$\mu^E = \mu_{exp}^E(x, T) = h(x) + Tg(x) \tag{17}$$

with empirical functions $h(x)$ and $g(x)$. However, the assumption of a linear dependence of μ^E on T can hardly be justified for the low temperatures $T = 310$–410 K studied in these experiments, and functions $h(x)$ and $g(x)$ cannot be considered as the partial enthalpy and entropy of hydrogen (II). Therefore, we suppose relation (17) to be only an empirical interpolation for $\mu^E(x, T)$ in the limited interval of T considered. In figure 4 we compare our microscopic expressions (4)–(10) for μ^E in this interval with the experimental $\mu_{exp}^E(x, T)$. We see that for $x \leqslant 0.83$ the model $\mu^E = \mu_0^E$ chemical potential calculated with $h_{ti} = h_\alpha(x)$ and $\gamma_i = \gamma_i^0$ (curve B in figure 4) agrees satisfactorily with μ_{exp}^E (and it is also true for $\gamma_i = \gamma_i^1$). Taking into account the extreme simplicity of the model, the agreement may be considered as confirmation of the concepts used. At the same time, curve E in figure 4, calculated without the $\mu_{ci}^E(x)$ term in (13), disagrees sharply with the experiment, which illustrates the importance of the $\mu_{ci}^E(x)$ contribution for realistic descriptions of $\mu(x, T)$.

For larger $x > 0.83$ the dependence of μ_{exp}^E on x (figure 4) has an inflection point and deviates from μ_0^E. This may be due to one more change in the character of the band structure. For example, the calculations of Ho *et al* (1984) for stoichiometric β-NbH imply that at $x \sim 0.8$–0.9 the Fermi level can fall off to a pronounced Van Hove type minimum in the electron state density. To estimate $h_{ti}^E(x)$ for $x > 0.83$, we use the $\mu_{exp}^E(x, T_2)$ values from (17) at the average experimental temperature $T_2 = 360$ K of

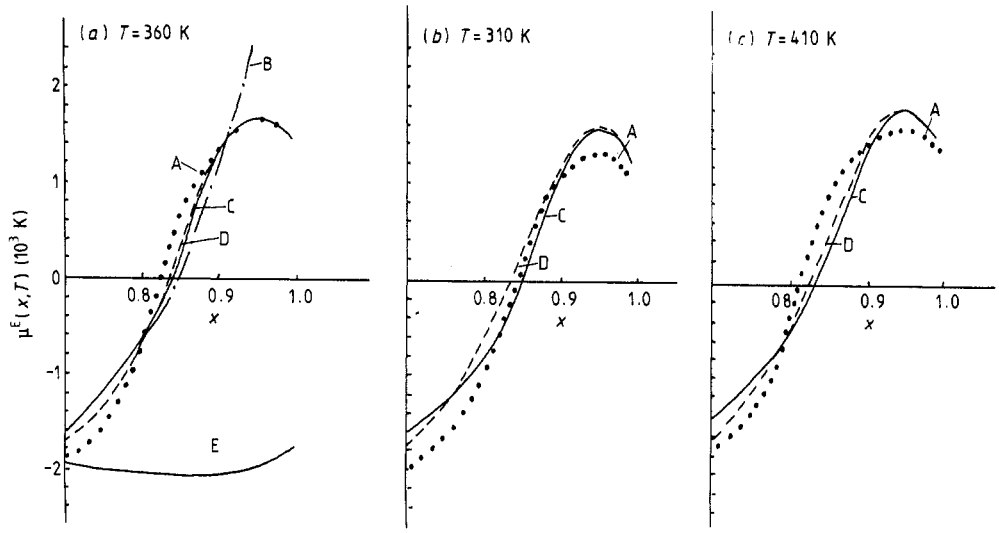

Figure 4. Excess chemical potential of hydrogen, $\mu^E(x, T)$ (equation (12)), in the β phase of NbH_x at different T. Curve A (dotted) presents μ^E_{exp} (Kuji and Oates 1984b). Curves B–E show μ^E calculated with different h^E_{ti} from (13) and γ_ξ, γ_ρ from (8): B, $h^E_{ti} = h_\alpha$, $\gamma_\xi = \gamma^0_\xi$, $\gamma_\rho = \gamma^0_\rho$; C, model F; D, model G; E, $\gamma_\xi = \gamma^0_\xi$, $\gamma_\rho = \gamma^0_\rho$, $h^E_{ti}(x) = \mu^{mf} = \gamma_\alpha x$ with γ_α from (11).

Kuji and Oates (1984b). We suppose that for $x > 0.9$ the difference between $\mu^E_{exp}(x, T_2)$ and $\mu^E_0(x, T_2)$ (or $\mu^E_1(x, T_2)$ calculated with $h_{ti} = h_\alpha$, $\gamma_i = \gamma^1_i$) is determined only by the sought-for $h^E_{ti}(x)$ function, while between $x = 0.83$ and $x = 0.9$ it smoothly matches the $h_\alpha(x)$ function from II. This yields the following form of h^E_{ti} (in K):

$$h^E_{ti}(x) = \begin{cases} h_\alpha(x) - 970(x - 0.83)^2\theta(x - 0.83) & x < 0.9 \\ \mu^E_{exp}(x, T_2) - [\mu^E_{0.1}(x, T_2) - h_\alpha(x)] & x > 0.9 \end{cases} \tag{18}$$

The accuracy of the resulting description of $\mu^E_{exp}(x, T)$ (including also the modifications of $\gamma_i(x)$, according to the relations (19) discussed below) is illustrated by curves C and D in figure 4 and can be treated as satisfactory.

It turns out, however, that the modification (17) of $h^E_{ti}(x)$ at large x has little effect on the α'–β PT considered. The phase equilibrium curves calculated with $h^E_{ti}(x)$ from (18) for all $x \leqslant 0.9$ almost coincide with those shown in figure 3(*a*). Thus the correction (18) does not eliminate the above disagreement with experiments in the shape of $T_i(x)$ at large x.

Let us now discuss the effects of the concentration dependence of the parameters γ_i in (8). Taking into consideration the mentioned manifestations of the band-structure effects in NbH_x, the presence of such a dependence seems to be quite natural. However, in the absence of microscopic calculations, it can be introduced only phenomenologically. Experiments show that characteristic points for the concentration dependence of H–H interactions in NbH_x are $x \simeq 0.6$ and $x \simeq 0.83$ (see II and figure 4). Therefore, we suppose the following model form for $\gamma_i(x)$:

$$\gamma_i(x) = \gamma_i + b_i(x - 0.6)^2\theta(x - 0.6) - d_i(x - 0.83)^2\theta(x - 0.83). \tag{19}$$

Let us note that when γ_i depends on x, additional terms arise in relations (8*b*) for μ^{mf}_λ in

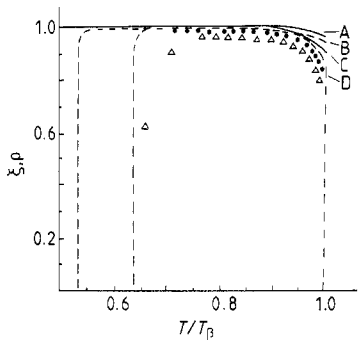

Figure 5. Dependence of the order parameters in the β phase of NbH_x at $x = 0.83$ on the reduced temperature, T/T_β, where T_β is the transition temperature to the homogeneous β phase. Experiments: full circles correspond to the reduced tetragonal strain $U(T)/U(250\ K)$ with the values of $U = U_{zz} - U_{xx}$ taken from figure 2.14 of Shober and Wenzl (1978); open triangles are the values of $I^{1/2}(T)/I^{1/2}(250\ K)$, where $I(T)$ is the intensity of the superstructure reflections estimated from figure 7 of Welter and Schöndube (1983). Notations for theoretical curves are as follows: A, $\xi(T)$ taken from model G; B, $\rho(T)$ from model G; C, $\xi(T)$ from model F; D, $\rho(T)$ from model F.

accordance with the thermodynamic relation (6*b*). The correction $\delta\mu_\lambda^{mf}$ is the same for all λ = a, b, α and is

$$\delta\mu_\lambda^{mf} = \sum_i \frac{\partial F}{\partial \gamma_i}\frac{\partial \gamma_i}{\partial x} = 6c^2\left(\xi\frac{\partial \gamma_\xi}{\partial x} + \tfrac{3}{2}\rho^2\frac{\partial \gamma_\rho}{\partial x}\right). \tag{20}$$

To illustrate qualitatively the effects of the modifications of the dependence (19) on the PT, we present in figure 3(*d*) $T_i(x)$ calculated by using expressions (18)–(20), $\gamma_i = \gamma_i^0$ at $d_i = 0$ and at several values of $b_\xi = b_\rho$ in equation (19). We see that when b_i increases, i.e. $|\gamma_i|$ decreases, the PT temperatures $T_i(x)$(are, naturally, lowered and the phase diagrams become similar to the observed one. By varying the b_i and d_i values in (18), we can change the details of the $T_i(x)$ dependences.

In what follows we shall consider two representative models determined by relations (4)–(10) and (18)–(20). The first one corresponds to the values $\gamma_i = \gamma_i^0$, $d_i = 0$, $b_\xi = b_\xi^0 = 5000$K, $b_\rho = b_\rho^0 = 1000$ K in (19) and will be called model F (to distinguish it from models A–E in II). Figure 1 shows that the phase diagram in this model is similar to that suggested by Shober and Wenzl (1978). The second one, called model G, corresponds to the values $\gamma_i = \gamma_i^1$, $b_\xi = b_\rho = 5000$ K, $d_\xi = d_\rho = 14\,000$ K. The phase diagram for this model in figure 1 at large x resembles that suggested by Welter and Shöndube (1983); in particular, the point of equal concentrations $x_{\alpha'}(T) = x_\beta(T)$ is present. For the $\alpha(\alpha')$ phase at $x < 0.83$ both the models coincide with model A from II. Let us also note that total variations $\Delta\gamma$ of parameters $\gamma_i(x)$ in (19) for all values $x \leqslant 0.9$ considered are not large: $|\Delta\gamma_i/\gamma_i| \leqslant 0.2$. Therefore, comparison of figures 3(*a*), 3(*d*) and 1 illustrates the sensitivity of the detailed form of phase diagrams to a relatively weak concentration dependence of $\gamma_i(x)$. At the same time the main features of the observed phase diagram are described even by simple models with concentration-independent γ_i (figure 3(*a*)) and are determined by the discussed sharp increase of $\partial\mu/\partial x \simeq \partial h_\alpha/\partial x$ at $x \geqslant 0.6$.

4. Characteristics of β ordering in NbH_x

In this section we discuss the results of calculations for the main characteristics of the β ordering in NbH_x. The results are not too sensitive to details of the models and those for models F and G defined above will be presented.

In figure 5 we present the order parameters $\xi(T)$ and $\rho(T)$ for NbH_x at $x = 0.83$. Experimentally, the parameters can be estimated from data on the tetragonal strain $U =$

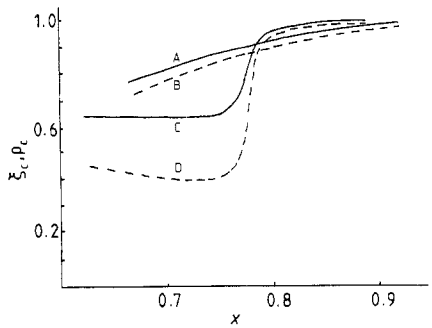

Figure 6. Calculated jumps of the order parameters $\xi_c(x)$ and $\rho_c(x)$ in NbH_x as defined in (21). Notations for curves are as follows: A, $\xi_c(x)$ taken from model G; B, $\rho_c(x)$ from model G; C, $\xi_c(x)$ from model F; D, $\rho_c(x)$ from model F.

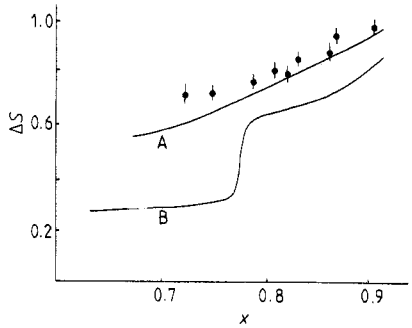

Figure 7. Entropy of the α'–β transition, $\Delta S(x)$, in NbH_x, as defined in (22). Experimental points are taken from figure 2.16 of Schober and Wenzl (1978). Theoretical curves: A, model G; B, model F.

$U_{zz} - U_{xx}$ in the β phase, since in the linear-in-U approximation, U is proportional to ξ (V). The quantity ρ is the amplitude of the CW ρ (in (2)) with the superstructure vector $\boldsymbol{k}_1$, and the intensity of the superstructure reflections, $I(T)$, is proportional to ρ^2. Therefore, for comparison with the calculations in figure 5, we present the experimental values of $U(T)/U(T_0)$ estimated from the data of Pick cited by Shober and Wenzl (1978) as well as those of $I^{1/2}(T)/I^{1/2}(T_0)$ estimated from the data of Welter and Schöndube (1983). Here $T_0 \simeq 250$ K is the temperature at which $U(T)$ and $I(T)$ are close to the respective saturation values. It is seen that the calculations agree qualitatively with experiments. Let us also note that at $T \leqslant 250$ K the calculated $\rho(T)$ drops and the CW disappears from the ordering. This correlates qualitatively with the experimental fall of $\rho(T)$, which is shown in figure 5 and is connected with the PT to another phase.

In figure 6 we show the calculated jumps of the order parameters for the α'–β PT, i.e. the values of $\xi = \xi_c(x)$ and $\rho = \rho_c(x)$ on the phase equilibrium curve $T_\beta = T_\beta(x)$:

$$\xi_c(x) = \xi(x, T) \qquad \rho_c(x) = \rho(x, T). \tag{21}$$

Each curve in figure 6 starts from the value $x = x_\beta(T_t)$ corresponding to the calculated triple point temperature T_t. In figure 7 values of the transition entropy $\Delta S(x)$ are presented:

$$\Delta S(x) = S_{\alpha'}(x, T_{\alpha'}(x)) - S_\beta(x, T_\beta(x)). \tag{22}$$

A prominent feature of the concentration dependences $\xi_c(x)$, $\rho_c(x)$ and $\Delta S(x)$ in figures 6 and 7 is a sharp step-like rise of the parameters at some x in model F (and also in other models with not large $|\gamma_i| \leqslant |\gamma_i^0|$). Generally, an increase of the order parameters with x for a given T is due to the rise of the ordering energy with x, e.g. in (8*a*), as compared with the counter-acting entropic terms, e.g. in (7). An increase of $T_\beta(x)$ with x can prevent this rise and this is the case for the initial parts of the curves in figure 6. However, when $T_\beta(x)$ becomes almost horizontal and initial values of ξ_c, ρ_c and ΔS are not large, they grow very sharply at a certain x. In model G (and others with large $|\gamma_i| \geqslant |\gamma_i^1|$) values of ξ_c, ρ_c are large and close to saturation even near $x_\beta(T_t)$. Thus their rise with x is much smoother and the step-like behaviour is not pronounced.

The comparison with the experimental $\Delta S(x)$ in figure 7 shows that $\Delta S(x)$ values calculated in model G agree with the data much better than those in model F: only a

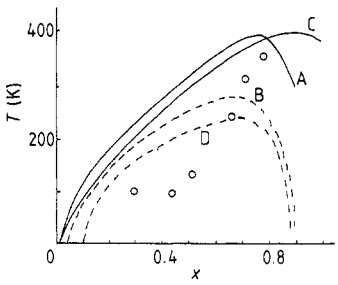

Figure 8. Instability temperature, $T_{\xi}(x)$ or $T_{\rho}(x)$, of the disordered α phase in NbH_x with respect to creation of the ξ or ρ CW. Experiments: open circles denote $T_{\xi}(x)$ estimated as described by Vaks *et al* (1988a) from the data of Mazzolai and Birnbaum (1985) on the elastic constants. Theoretical curves: A, $T_{\xi}(x)$ taken from model G; B, $T_{\rho}(x)$ from model G; C, $T_{\xi}(x)$ from model F; D, $T_{\rho}(x)$ from model F.

slight break is seen in the data instead of the step-like behaviour. On the other hand, model F is better at describing the phase diagram in figure 1. Therefore, the models used cannot simultaneously describe details of the concentration dependences for both the phase equilibrium curves $T_i(x)$ and $\Delta S(x)$. This is, of course, quite possible for such simplified models. For example, the presence in the β phase of the dispersionless phonon-like excitations reported by Shapiro *et al* (1981) and neglected in our models may have some effect on $\Delta S(x)$. Thus direct measurements of order parameters $\xi_c(x)$, $\rho_c(x)$ as well as more thorough investigations of $\Delta S(x)$, $S_{\alpha}(x, T)$ and $S_{\beta}(x, T)$ in NbH_x (in particular, at not large $x < 0.75$) appear to be desirable.

In figure 8 we present the 'ordering spinodals' (De Fontaine 1979), i.e. the temperatures $T_{\xi}(x)$ or $T_{\rho}(x)$ at which the disordered α phase becomes unstable with respect to the creation of the ξ or ρ CW of an arbitrarily small amplitude (V). The experimental $T_{\xi}^{exp}(x)$ values are also shown, which were estimated in V from the data of Mazzolai and Birnbaum (1985) on the anomalies of the elastic constants $C_{ij}(T, x)$ in the α phase of NbH_x near temperatures of the PT to the β phase. A comparison with figure 3 in V shows that $T_{\xi}(x)$ values in models F and G agree with $T_{\xi}^{exp}(x)$ better than those in model A in V, and at not small $x \geqslant 0.7$ T_{ξ} and T_{ξ}^{exp} are close. At smaller x the agreement worsens but experimental errors in $T_{\xi}^{exp}(x)$ become much larger here. Figure 8 also shows that values of $T_{\rho}(x)$ are lower than $T_{\xi}(x)$ and are significantly spaced apart from the PT temperatures $T_{\alpha'}(x)$. This agrees qualitatively with the lack of evidence for pretransition phenomena connected with the CW ρ in the α' phase of NbH_x (Welter and Schöndube 1983) while the mentioned anomalies in $C_{ij}(x, T)$ connected with the CW ξ (V) are rather pronounced (Mazzolai and Birnbaum 1985).

Since all the main properties of $Nb(H,D)_x$, $Ta(H,D)_x$ and VD_x in the α phase are similar in experiments (Shober and Wenzl 1978, Somenkov and Shilstein 1980) as well as in models (II, Futran *et al* 1982), it is natural to suppose that near the α–δ PT in TaH_x and VD_x the ξ CW is also much softer than the ρ CW. Then the sharp rise of the specific heat observed by Voronel *et al* (1968) near the α–δ PT in $VD_{0.8}$ should be due to the fluctuation effects connected with the ξ CW. Therefore, we expect that the effects of the pretransitional softening and relaxation in the shear constant $C' = \frac{1}{2}(C_{11} - C_{12})$ discussed in V (but not in the constant C_{44} and bulk modulus B) should be still sharper and more pronounced in VD_x than those seen by Mazzolai and Birnbaum (1985) in NbH_x. Experimental verification of this prediction would be an important test for the discussed concepts on hydrogen ordering in hydrides.

5. Conclusions

Let us summarise the main results of this work. First, this and the preceding work (II, VI) illustrate the scope for and limitations of conventional models with pairwise

interactions in describing real interstitial alloys. As is noted in II and above at not large concentrations $x \leqslant 0.5$, models with pairwise concentration-independent $V_{HH} = V_{sr} + V_{si} + V_e$ describe the thermodynamics and α–α' PT in NbH_x fairly well. However at $x \geqslant 0.6$ sharp concentration dependences of properties are manifested, which appear to be due to significant changes of the electronic state of hydrogen in NbH_x. Even qualitative features of the observed phase diagrams cannot be understood without allowance for these effects. It is natural to expect that these non-pairwise band-structure effects are also characteristic of other interstitial alloys. As has been mentioned, one of the indications of that may be the stability of many ordered interstitial metal–non-metal alloys even at large deviations from stoichiometry (Goldschmidt 1967). Our consideration shows, however, that even phenomenological allowance for these effects can be sufficient for understanding the main features of the PT and phase diagrams. In II and in this work it was done by using the estimates of the configuration- and temperature-independent contributions $h_{ti}(x)$ to the chemical potential of hydrogen from the experimental data on its solubility in NbH_x(Kuji and Oates 1984a, b). It is also shown in II and in this work that in the configuration-dependent contributions to thermodynamic potentials the non-pairwise concentration-dependent effects are apparently not large.

Treating the mean-field constants γ_ξ and γ_ρ in (8) as free parameters of the model (i.e. using them for simulating disregarded effects), we have described the main features of the α–α'–β phase diagram in NbH_x (see figure 3(*a*)). The fitted values of γ_ξ are close to that calculated in the model estimate (11) while the value of $|\gamma_\rho|$ in the model estimate appears to be underestimated. The addition of relatively small concentration-dependent terms to γ_ξ and γ_ρ, according to (19) (with the same type of x dependence as that estimated from the experiments for $h_{ti}(x)$), enables us also to explain the peculiar form of the phase equilibrium curves $T_{\alpha'}(x)$ and $T_\beta(x)$ in NbH_x at large $x \geqslant 0.75$ (figure 1). We calculated the chemical potential in the β phase (figure 4), the temperature dependences of the order parameters (figure 5), the transition entropy in model G (figure 7) and the ordering spinodal $T(x)$ for the CW (figure 8) and revealed fair agreement with the experiments.

The results obtained enable us to make a number of qualitative predictions about properties of hydrides under consideration. We suppose that the stability of the δ phase in TaH_x and VD_x in a very broad range of x has the same 'electronic' origin as that for the β phase of NbH_x. Then the concentration anomalies in the α phase at $x \geqslant x_s \simeq 0.6$ discussed in II for NbH_x are also expected for TaH_x and VD_x, such as the sharp rise of the chemical potentials μ and $\partial\mu/\partial x$, the maxima in the electrical resistivity $\rho(x)$ near x_s, anomalies in the thermo-power at $x \sim x_s$, etc. We predict the pretransitional softening of the shear constant $C'(x, T)$ in the α phase of TaH_x and VD_x which should still be sharper in VD_x than that observed in NbH_x. The 'step-like' dependences for the order parameters $\xi_c(x)$ and $\rho_c(x)$ on the curve $T(x)$ (of the type shown by curves C and D in figure 6) are also possible. The predictions seem to be insensitive to the details of the models, being connected mainly with the general concepts on the PT considered. Therefore their experimental verification seems to be interesting and useful for the development of microscopic theories of hydrides as well as other interstitial alloys.

Acknowledgments

The authors are much indebted to V G Orlov for participation at the initial stage of this work, to Mrs N B Levchuk for technical assistance and also to N E Zein for useful discussions.

References

De Fontaine D 1979 *Solid State Phys.* **24** 73
Futran M, Coates S C, Hall C K and Welch D O 1982 *J. Chem. Phys.* **77** 6223
Goldschmidt H J 1967 *Interstitial Alloys* vols 1 and 2 (London: Butterworths)
Hall C K, Soteros G, McGillifray I and Shirley A I 1987 *J. Less-Common Met.* **130** 319
Ho K-M, Tao H-J and Zhu X-Y 1984 *Phys. Rev. Lett.* **53** 1586
Horner H and Wagner H 1974 *J. Phys. C: Solid State Phys.* **7** 3305
Khachaturian A G 1974 *Theory of Phase Tranformations and Structure of Solid Solutions* (Moscow: Nauka)
Kikuchi R 1951 *Phys. Rev.* **81** 988
Köbler V and Welter J-M 1982 *J. Less-Common Met.* **84** 225
Kuji M and Oates W A 1984a *J. Less-Common Met.* **102** 251
—— 1984b *J. Less-Common Met.* **102** 261
Mazzolai F M and Birnbaum H K 1985 *J. Phys. F: Met. Phys.* **15** 507, 525
Richards P M 1983 *Phys. Rev.* B **28** 300
Shapiro S M, Richter D, Noda Y and Birnbaum H 1981 *Phys. Rev.* B **23** 1594
Shober T and Wenzl H 1978 *Hydrogen in Metals* vol. 2, ed. G Alefeld and J Völkl (Berlin: Springer)
Somenkov V A and Shilstein S S 1980 *Prog. Mater. Sci.* **24** 267
Vaks V G and Orlov V G 1986 *Fiz. Tverd. Tela* **28** 3627
—— 1988 *J. Phys. F: Met. Phys.* **18** 883
Vaks V G and Zein N E 1987 *Fiz. Tverd. Tela* **29** 68
Vaks V G, Zein N E and Kamyshenko V V 1988a *J. Phys. F: Met. Phys.* **18** 1641–61
Vaks V G, Zein N E, Kamyshenko V V and Tkachenko Yu V 1988b *Fiz. Tverd. Tela* **30** 477
Vaks V G, Zein N E, Zinenko V I and Orlov V G 1984 *Sov. Phys.–JETP* **87** 2030
Voronel A V, Garber S R and Mamnitsky V M 1968 *Sov. Phys.–JETP* **55** 2017
Welter J-M and Schöndube F 1983 *J. Phys. F: Met. Phys.* **13** 529